Physics of Plasmas

Measurement of the Taylor scale in a magnetized turbulent laboratory plasma wind-tunnel

Cite as: Phys. Plasmas **29**, 032305 (2022); https://doi.org/10.1063/5.0073207
Submitted: 28 September 2021 • Accepted: 23 February 2022 • Published Online: 08 March 2022

C. A. Cartagena-Sanchez, J. M. Carlson and D. A. Schaffner

Physics of Plasmas ARTICLE scitation.org/journal/php

Measurement of the Taylor scale in a magnetized turbulent laboratory plasma wind-tunnel

Cite as: Phys. Plasmas **29**, 032305 (2022); doi: 10.1063/5.0073207
Submitted: 28 September 2021 · Accepted: 23 February 2022 ·
Published Online: 8 March 2022

C. A. Cartagena-Sanchez,[a] J. M. Carlson, and D. A. Schaffner

AFFILIATIONS

Department of Physics, Bryn Mawr College, Bryn Mawr, Pennsylvania 19010, USA

[a]Author to whom correspondence should be addressed: cacsphysics@gmail.com

ABSTRACT

The fluid Taylor scale is measured in the Bryn Mawr Experiment (BMX) of the Bryn Mawr Plasma Laboratory and examined as a potential dissipation scale of magnetic turbulence within the plasma. We present the first laboratory measurements of the Taylor scale of a turbulent magnetized plasma through multi-point correlations of broadband magnetic fluctuations. From spatial and temporal correlations, respectively, the measured Taylor scales are 2 ± 1 and 3 ± 1 cm. These measurements are on the same order of magnitude as estimated ion dissipation scales within the BMX plasma with ion inertial scales between 1 and 10 cm and ion gyroscales between 0.1 and 1.0 cm. From these measurements, a magnetic Reynolds number can be computed. Since Taylor scale values are determined using multi-point correlations and a Richardson extrapolation technique, an estimate of the magnetic Reynolds number can be found without the added complication of specifying a model of microscopic diffusivity, a parameter often difficult to obtain experimentally.

I. INTRODUCTION

Spatial velocity correlation functions have been measured in conventional fluid turbulence for decades,[1–4] but spatial magnetic correlations in turbulent plasmas are less common. Spatial measurements of the magnetic correlation function in the solar wind plasma were studied by Matthaeus *et al.*.[5] They used simultaneous magnetic field data from several spacecraft, including the four Cluster spacecraft in tetrahedral formation. The measurements were performed with separations ranging from 150 to 2.2×10^6 km ($350 R_E$). From measurements of the correlation length and the Taylor scale, 2478 ± 702 km, they report an effective magnetic Reynolds number of the solar wind $R_{mT} = 230\,000$.

In follow-up papers, Weygand *et al.*[6–9] modified and improved the earlier result. Weygand *et al.*[6] introduce a modification to the analysis by using a Richardson-extrapolation method, which probes the trends of fits as the separation shrinks from 10^6 to 100 km to extrapolate the Taylor scale at zero-separation. They report a Taylor scale of 2400 ± 100 km. This measurement confirms the earlier work,[5] and they find a solar wind magnetic Reynolds number of $R_{mT} = 260\,000 \pm 20\,000$. In addition, using magnetospheric plasma sheet (tailward of Earth) data, they measure a Taylor scale of 1900 ± 100 km and find a smaller Reynolds number $R_{mT} = 111 \pm 12$, due mostly to the smaller correlation length found in the plasma sheet. Anisotropies in the correlation function parallel and perpendicular to the local magnetic field have also been studied,[7–9] and Taylor scales parallel to the local field in the intermediate ($600\,\text{km/s} \geq \text{speed} \geq 450\,\text{km/s}$) solar wind are found to be longer than perpendicular to the field. Weygand *et al.* in 2011[9] report a Taylor scale of 3500 ± 500 km parallel and 1200 ± 500 km perpendicular to the local magnetic field in the intermediate solar wind. In the slow ($\textit{speed} \leq 450$ km/s) solar wind, they find a Taylor scale of 1200 ± 100 km with no variation between parallel and perpendicular to the local magnetic field.

Recently, Bandyopadhyay *et al.*[10] explored spatial magnetic correlations with data from the Magnetospheric Multiscale (MMS) mission. They augment previous work[5,6] with smaller separations, 25 km $\leq r \leq$ 200 km, and a bead-like spacecraft alignment (in contrast to tetrahedral formation). They obtain a Taylor scale of ~7000 km in the solar wind.

Measurements of such a Taylor scale have not yet been conducted in a laboratory version of a magnetically turbulent plasma, in part due to the difficulty of recreating similar turbulent conditions in the lab as can be found in space or astrophysical settings. Work on the Swarthmore Spheromak Experiment (SSX) has shown that broadband magnetic fluctuations can be generated using a plasma gun to launch magnetic structures into a wind tunnel-like flux-conserving column.[11–14] The Bryn Mawr Experiment (BMX) at Bryn Mawr College has been constructed to expand upon these experiments and continue exploring heliospheric-relevant magnetic turbulence in the laboratory.

This paper presents measurements of the spatial and temporal correlations of fluctuating magnetic fields within the BMX plasma wind tunnel. These correlation functions allow for an extrapolated zero-separation Taylor scale measurement following the Richardson-extrapolation method introduced in Weygand *et al.*.[6] An estimate of the correlation scale is also made using these correlation functions. Finally, with both a correlation scale and a Taylor scale, a prediction of the magnetic Reynolds number is made. This approach for determining a magnetic Reynolds number relies only on directly measured data and avoids the need to specify a model for microscopic diffusivity (commonly based on Spitzer resistivity, for example), which is difficult to measure accurately and requires many different diagnostics.

II. TECHNIQUE

The magnetic Reynolds number is a dimensionless quantity relating the large-scale current flows to the energy dissipated via resistivity within a magnetofluid.[11] The magnetic Reynolds number is

$$R_m = \frac{\mu_o V L}{\eta}, \tag{1}$$

where V and L are the velocity and length scale associated with energy injection into the system, while η is the resistivity of the magnetofluid. The resistivity must be obtained through some model, which typically requires measurement or knowledge of both density and temperature. Alternatively, an effective magnetic Reynolds number can be constructed by following the dimensional analysis in fluid turbulence.[1,2] An analog of the fluid Reynolds number is formed for the magnetic Reynolds number,

$$R_m^{eff} \sim \left(\frac{\lambda_c}{l_k}\right)^{4/3}; \tag{2}$$

where λ_c and l_k are the correlation scale and the Kolmogorov scale, respectively. The correlation scale represents the energy-containing scale, and the Kolmogorov scale is the dissipation scale associated with critically damped fluctuations.[10]

Attempting to connect the Kolmogorov scale to a particular dissipation mechanism within plasmas is difficult because these systems have varying degrees of collisionality, leading to alternative dissipative mechanisms beyond collisional resistivity. Mirco-magnetic reconnection[15] and ion-cyclotron resonance heating[16] are two examples of such mechanisms[17] found in weakly collisional or collisionless plasmas common in astrophysical settings. Though the plasma found in BMX is likely more collisional than space or astrophysical plasmas, this paper remains agnostic as to the mechanism for dissipation, adopting instead the Taylor scale, λ_T, as the dissipation scale as it can be determined directly from the experimentally measured quantities.

In a hydrodynamic ordered plasma,[18] $\lambda_T > l_k$, the Taylor scale is the spatial length at which dissipation begins to affect the fluctuations. The Taylor scale and the Kolmogorov scale are related to the magnetic Reynolds number[18] $\lambda_T/l_k = R_m^{1/4}$. The accessibility of the Taylor scale, from spatial magnetic correlations,[19] motivates its use in defining the effective magnetic Reynolds number. The effective magnetic Reynolds number recast in terms of the correlation scale and the Taylor scale is

$$R_m^{eff} \sim \left(\frac{\lambda_c}{\lambda_T}\right)^2. \tag{3}$$

A. Spatial magnetic correlations

A spatial magnetic correlation is the cross correlation between two magnetic data time-series recorded simultaneously, but at separate locations. The value of the cross correlation at zero-time delay is taken for different values of separation, r, to generate a spatial correlation function defined as

$$R(\vec{r}) = \frac{\vec{b}(t)\cdot\vec{b}(t,\vec{r})}{\sigma_t \sigma_{t,\vec{r}}}. \tag{4}$$

The $\langle\cdots\rangle$ represents a time average, $\vec{b}$ represents mean-subtracted magnetic fluctuations, $\vec{r}$ is the probe-separation vector, and the normalization factor $\sigma_{t,\vec{r}}$ is the standard deviation of the mean-subtracted magnetic fluctuations at position $\vec{r}$.

In well behaved turbulence,[2] the spatial correlation function vanishes at large separations. To quantify the energy-containing scale, the correlation scale is used,

$$\lambda_c = \int_0^\infty R(\vec{r})dr. \tag{5}$$

Under the assumption that the turbulence is homogenous and isotropic,[20,21] the spatial correlation function takes a Gaussian-like form. Then, given the quadratic small-separation behavior of a Gaussian, and, thus, the spatial correlation function, a model for the Taylor scale can be obtained as

$$R(\vec{r}) \approx 1 - \frac{1}{2\lambda_T^2} r^2. \tag{6}$$

The Taylor scale is associated with the curvature of the spatial correlation function at zero-separation. In plasma turbulence, the Taylor scale is also associated with the mean square derivatives of the magnetic fluctuations, i.e., the thickness of a typical current layer,[5]

$$\lambda_T^2 \equiv \frac{\langle b^2\rangle}{\langle(\nabla\times\vec{b})^2\rangle}.$$

The normalized spatial correlation at small-separations Eq. (6) has spherical symmetry. In cylindrically symmetric cases, there is no difference in the functional form if the separation vector is along the axis of symmetry,[1] i.e., the $\hat{z}$-direction,

$$R(z) \approx 1 - \frac{1}{2\lambda_T^2} z^2. \tag{7}$$

This coordinate-invariance supports a linear or bead-like alignment for the probes in a cylindrically confined plasma, similar to the MMS alignment studied in Bandyopadhyay *et al.*.[10]

B. Temporal magnetic correlations

The spatial correlation function is limited by the spatial resolution between measurements. To interpolate between spatial points, an alternative approach is taken using the temporal correlation function at a single point and assuming that the Taylor Hypothesis[22] is valid—that temporal changes in the plasma are small compared to the rate that plasma advects past a measurement point. Through this hypothesis, single-point multi-time measurements are interpreted as multi-point snapshots. This temporal technique allows for the probing of

separations smaller than the minimum separation between two probes, which is currently limited by the vacuum chamber design.

A temporal magnetic correlation is the cross correlation between a time-series of magnetic data and its time-shifted copy. All portions of the two signals that do not overlap are zero-padded. For a given probe position, the temporal correlation function is defined as

$$R(\tau) = \frac{\langle \vec{b}(t) \cdot \vec{b}(t+\tau) \rangle}{\langle \sigma_t^2 \rangle}, \tag{8}$$

where τ is the time delay and σ_t^2 is the standard deviation of the mean-subtracted magnetic fluctuation. The $\langle \cdots \rangle$ is an average in t. $R(\tau)$ is converted to $R(z')$ by assuming $z' = \tau V_{bulk}$, where V_{bulk} is the bulk plasma speed.

III. THE BRYN MAWR EXPERIMENT (BMX)

Measurements of the Taylor scale are conducted within the Bryn Mawr Experiment (BMX). BMX consists of a cylindrical flux-conserving vacuum chamber with a magnetized plasma gun source (MPGS) at one end. Using a pulse-forming-network capacitor discharge, hydrogen gas is ionized between coaxial electrodes. The resulting magnetized plasma is launched into the chamber by $J \times B$ forces forming a plume of turbulent plasma wind within the tunnel.

A. Chamber and vacuum system

The full chamber is 270 cm in length with an inner diameter of 24 cm. The chamber is set to experimental vacuum pressure using a cryopump located near the midpoint of the length of the chamber. The base pressure for these experiments is about 1×10^{-7} Torr. The chamber has three sections: a copper section (the plasma source region, see Sec. III B), an aluminum flux-conserving diagnostic section (see Sec. III D), and a stainless steel flux-dissipating dump section.

B. Plasma source

As illustrated in Figs. 1(a) and 1(b), the MPGS consists of two concentric copper electrodes: The internal electrode has an outer diameter of 11 cm, and the external electrode has an inner diameter of 24 cm. The external electrode is part of the vacuum chamber. The stuffing threshold of a MPGS is obtained as $\lambda_{gun} = (1/r_{in})\sqrt{2/\ln(r_{out}/r_{in})}$, for the inner and outer radii of the gun.[23] For the gun dimensions on BMX, this yields a stuffing threshold of $\lambda_{gun} = 29\,\mathrm{m}^{-1}$.

Within the internal electrode, a 100-turn, $L = 329\,\mu$H copper coil generates a stuffing field. A crowbarred SCR-circuit pulses the coil with a 100 mF, 350 V capacitor bank producing up to $6mWb$ of magnetic flux through the cross section of the internal electrode.

Four Parker puff valves are evenly spaced around the external electrode. These valves introduce ultra-pure hydrogen gas into the chamber, are pressurized to 80 psi with a flow rate of $2.67 \times 10^{-3}\,\mathrm{cm}^3/\mathrm{ms}$, and are electronically opened or closed for a controllable amount of time. In these experiments, the valves are simultaneously opened for a duration of 9.5 ms injecting 1.32×10^{19} molecular hydrogen particles per shot. With the number of molecular

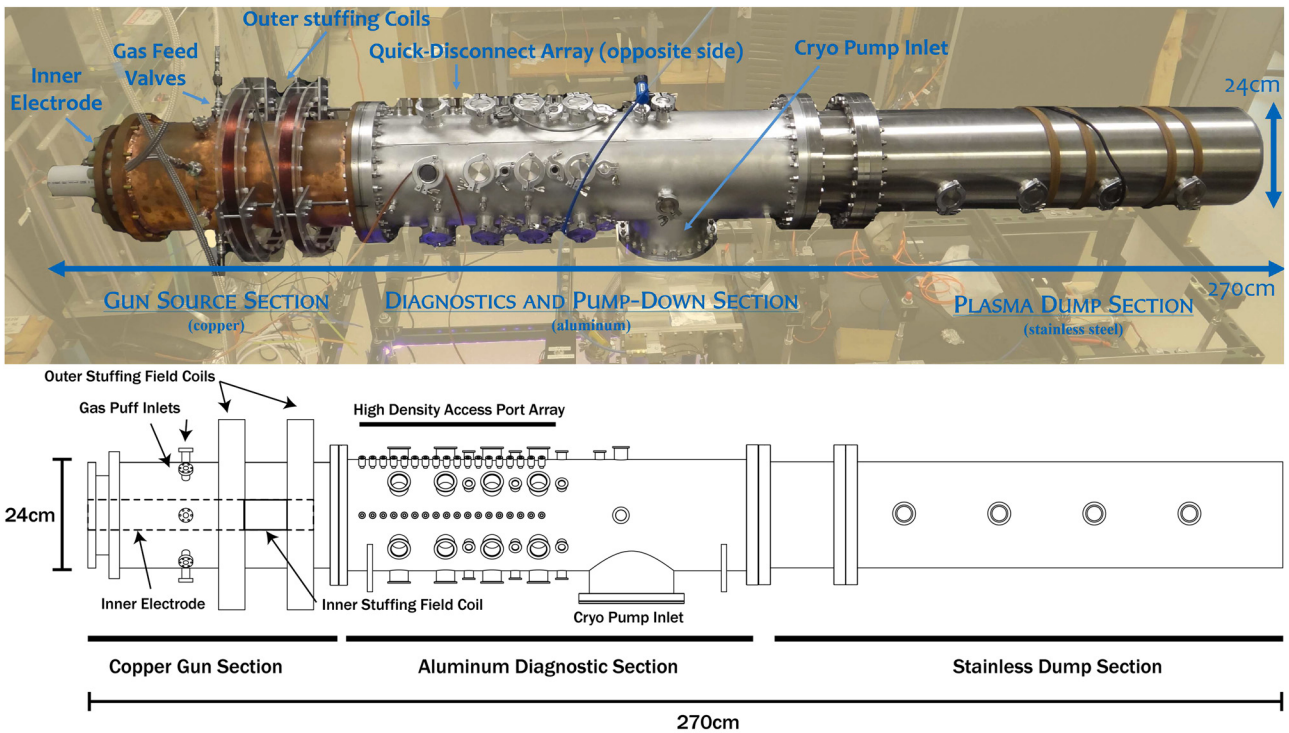

FIG. 1. An image(a) and diagram(b) of BMX.

hydrogen particles injected, the plasma density can be estimated. Assuming the injected gas is fully ionized and fills the chamber that the plasma density is $\lesssim 2.61 \times 10^{14}$ cm^{-3}.

C. Discharge circuit and plasma generation sequence

A pulse forming network (PFN) consisting of eight 0.5 mF oil-filled capacitors powers the plasma discharge. The PFN is discharged through a mercury ignitron switch. In these experiments, the banks are charged to 2 kV providing a total of 8 *k*J of stored energy per discharge. About 1.5 ms prior to triggering the ignitron switch, the inner stuffing coil engages, producing a pulse of magnetic flux within the gun over tens of milliseconds as shown in Fig. 2. The timing between stuffing coil and discharge sets the approximate background stuffing field for each shot—for these experiments, a 1.5 ms delay means that banks are triggered while flux is about 2 mWb. Similarly, 1 ms prior to the trigger, hydrogen gas is puffed and given time to fill the annular space between the electrodes. At ignitron trigger, the bank places the electrodes at the potential difference of the capacitor bank. The inner electrode is biased negatively with respect to the outer electrode. Once initial ionization occurs (within a few nanoseconds of trigger), current ramps up to a peak of about 70 kAmps as shown in Fig. 3(a). Simultaneously, the voltage across the electrodes settles to about 485 V as shown in Fig. 3(b). High current persists for approximately 180 ms.

D. Diagnostics

Single-loop three-axis magnetic wire coils (or b-dot probes) measure fluctuating magnetic fields. Each loop is wound on a 1/16 in. fiberglass stock and is inserted into a 1/4 in. glass tube. The glass tubes are inserted through quick disconnect ports spaced along the axis of the chamber at 2.6 cm intervals. For this experiment, eight probes are used simultaneously, where the first probe is 10.4 cm from the end of the inner electrode. The first two probes are removed from the analysis, due to the possibility that they measure a protruding stuffing field; hence, in this analysis, the third probe, at 15.6 cm from the end of the inner electrode, is the reference probe. To reduce stray pickup, the loop wires are twisted tightly using a wood-lathe for about three inches beyond the outside of the chamber and then converted to BNC coaxial cable to connect to the data acquisition units. The transition from twisted wire to BNC is covered in a copper tape to further reduce stray inductive and capacitive effects.

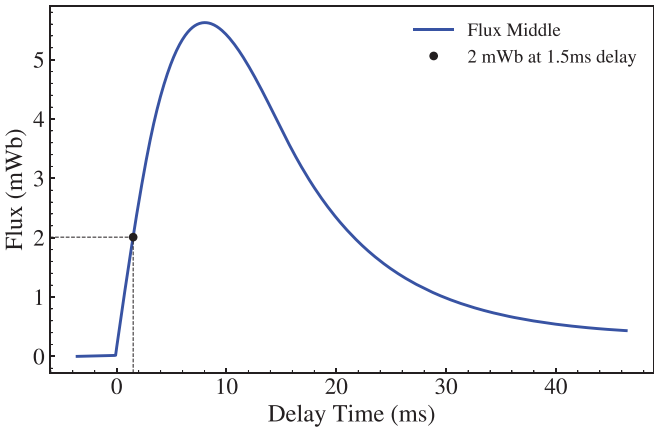

FIG. 2. Trace of magnetic flux as a function of delay time on BMX. A 1.5 ms delay time generates 2 mWb of flux at the plasma gun mouth. This flux injects helicity into the plasma at a rate of 0.97 Wb$^2/s$, given the 0.485 kV mean discharge voltage from Fig. 3(b).

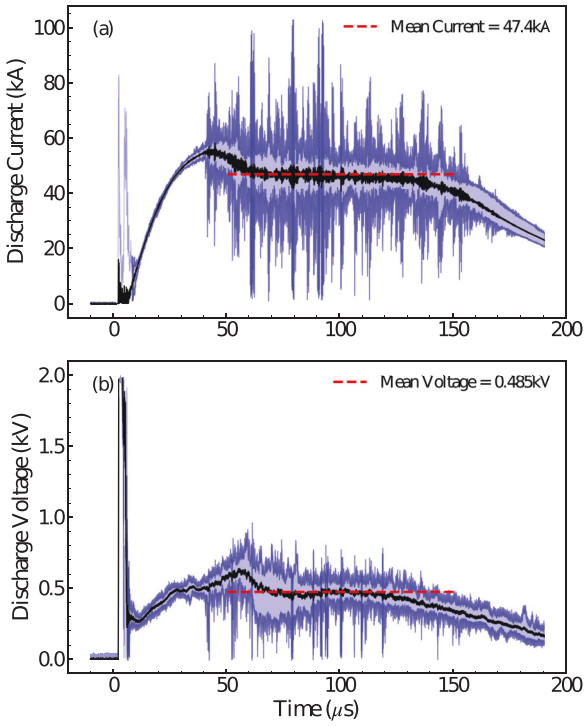

FIG. 3. The ensemble mean discharge current (a) and mean discharge voltage (b) with range of variation over all shots shaded. Dashed lines indicate mean current (47.4 kA) and mean voltage (0.485 kV) over a time interval of 50–150 μs.

A Power Electronics Measurements Rogowski Current Waveform Transducer placed at the source end of the PFN measures the discharge current. The discharge voltage is measured using a North Star High Voltage PVM-12 high frequency floating voltage probe.

E. Data acquisition

The three axes of each magnetic probe are organized in cylindrical coordinates $(\hat{r}, \hat{\theta}, \hat{z})$ and measure $d\vec{B}(t)/dt$ using a 14-bit, 100 MHz Picoscope Model 5443 with 50 Ω termination. The measurements are numerically integrated to construct a $\vec{B}(t)$ time series, as shown in Fig. 4. This data set is an ensemble of 25 bank discharges or shots. Figure 5 shows the probe-shot average magnetic power spectrum within a time window of $(75\ \mu s, 150\ \mu s)$ after the ignitron trigger.

F. Data processing

The $d\vec{B}(t)/dt$ data are integrated into $B(t)$, outlined in Sec. III E and filtered through a 30 kHz high-pass filter in software. Spatial and temporal correlations are then computed for the $(75\ \mu s, 150\ \mu s)$ time window. Within the same time window, the average time delay of prominent structures in the unfiltered magnetic field magnitudes,

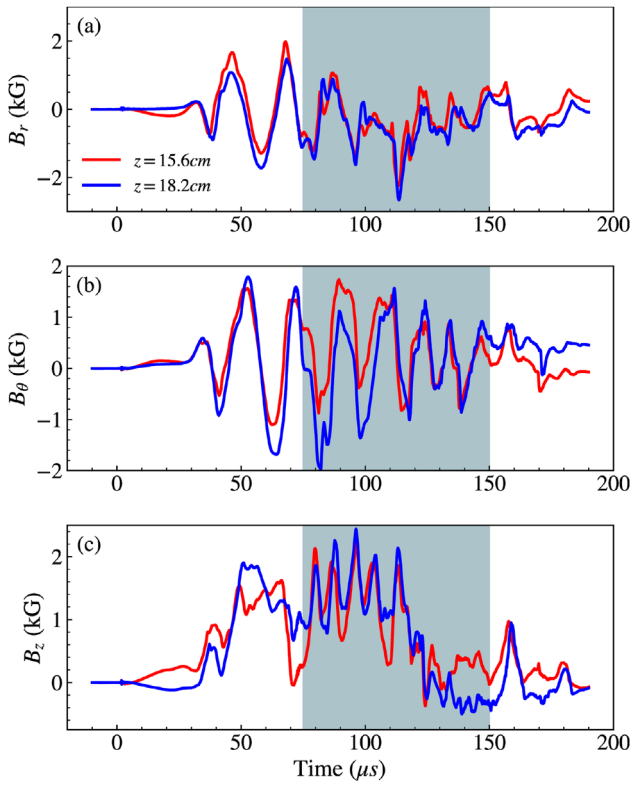

FIG. 4. The (a) r-component, (b) θ-component, and (c) z-component of the magnetic field for shot 23 measured $z = 15.6$ cm, in red, and $z = 18.2$ cm, in blue, from the inner electrode. The $(75\,\mu s, 150\,\mu s)$ epoch during which turbulent scales are investigated is highlighted.

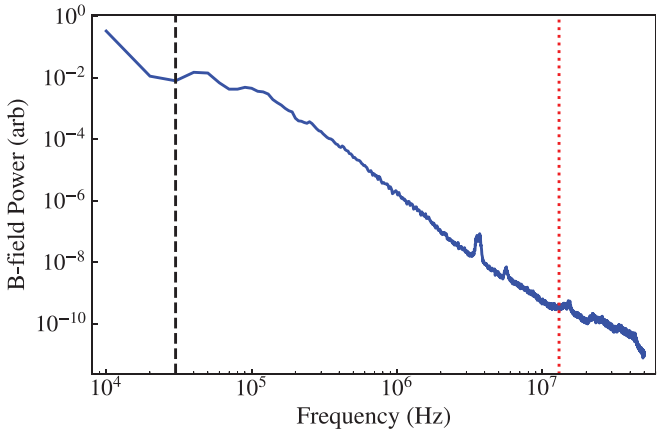

FIG. 5. The magnetic power spectrum averaged over all probes and shots at an injected helicity rate of 0.97 Wb^2/s resulting from 2 mWb of flux at the plasma gun mouth. The dashed line represents a 30 kHz high pass filter cutoff frequency, and the dotted line represents a 13 MHz ion cyclotron frequency.

$B_{mag}(t) = \sqrt{B_r^2(t) + B_\theta^2(t) + B_z^2(t)}$, is used to estimate the plasma bulk speed for each shot.

IV. RESULTS

A. Spatial correlation

Spatial correlations presented here are an accumulation of the modulus of probe-probe correlations. This approach can obscure anisotropic effects (such as differences between fluctuations parallel and perpendicular to the local field). However, this first step is justified as an initial analysis given the likelihood of a significant compressive component of the magnetic fluctuations. Work on SSX[14] has shown that magnetic turbulence generated in a similar manner as BMX contains a greater amount of compressive fluctuations compared to solar wind turbulence.[24]

Each probe-probe correlation is the cross correlation of the magnitude of the magnetic field fluctuations measured by each probe, i.e., $|b_{mag}(0)b_{mag}(z = 2.6n)|$. The integer n corresponds to the n^{th} probe away from the reference probe. For a single shot, the correlations are normalized by their respective zero-separated correlation, $R(0)$. The normalization scheme is chosen to isolate the turbulent fluctuations from that of any shot-to-shot variance in the plasma generation process.

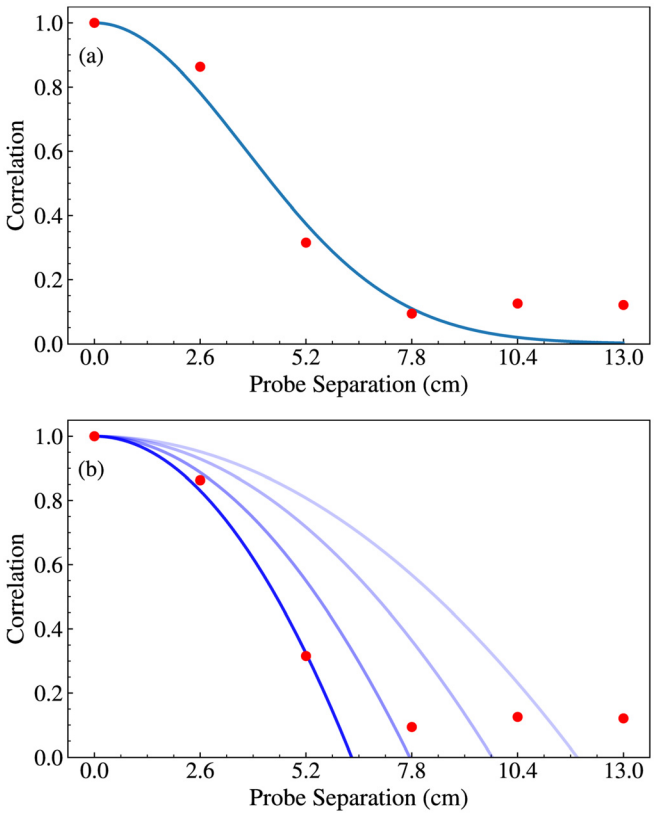

FIG. 6. The spatial correlation of b-field magnitude for shot 23 with, (a), the Gaussian fit of the shot used to compute the correlation scale and with, (b), the parabolic fits for the extraction of the Taylor scale through a Richardson extrapolation method.

Figure 6(a) shows the spatial correlation of shot 23. The spatial correlations show a Gaussian-like structure. A Gaussian, $e^{-z^2/2\sigma^2}$, is fit to the correlation function. The fit results in a Gaussian of width 3.7 ± 0.1 cm, which is then integrated using Eq. (5) from 0 to 18.2 cm—the space spanned by the probes—to compute a correlation scale of 4.6 ± 0.2 cm.

The spatial correlation is fit using Eq. (7) to determine the Taylor scale. However, this estimated Taylor scale is known to be affected by the maximum separation used.[3,6] Any Taylor scale computed directly from a correlation function is called a biased Taylor scale in this work. Following a similar procedure as in Weygand 2007,[6] the Taylor scale at zero separation, $\lambda_T(0)$, is extracted using a Richardson extrapolation method on the spatial correlation, minimizing the biasing effect. The method is a two-step procedure. First, an ordered-sequence of biased Taylor scales is generated, each element corresponding to fitting Eq. (7) to a subset of spatial correlation points, see Fig. 6(b). The sequence is ordered by the number of points included in the fit. Figure 6(b) shows the fits, and Fig. 7(a) shows the biased Taylor scales for each fit.

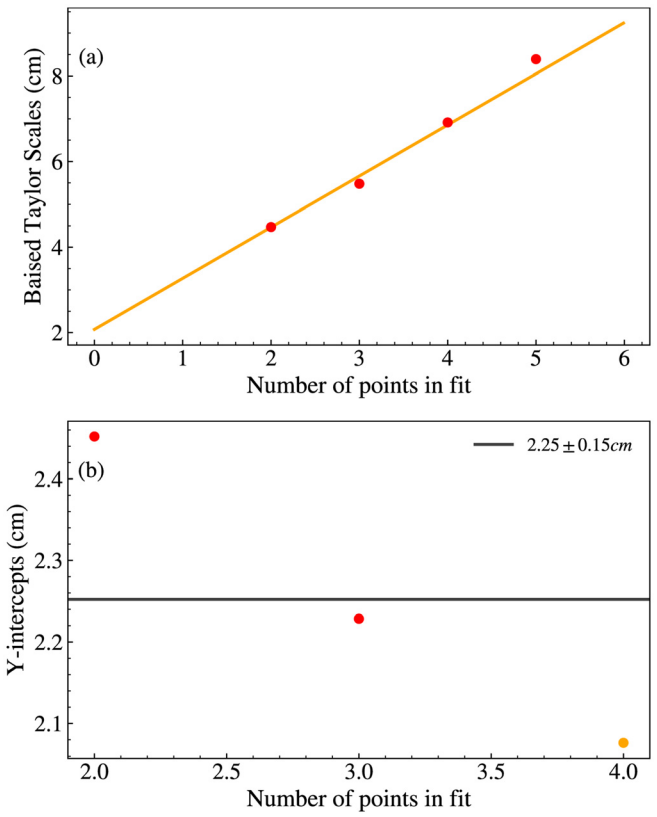

FIG. 7. The two-step Richardson extrapolation method first generates biased Taylor scales by fitting parabolas to the spatial correlation. The second step exploits the linear trends of the biased Taylor scales and extrapolates the y-intercepts. (a) Biased Taylor scales as a function of number of points used to fit the spatial correlation function. A linear fit is performed on all the biased Taylor scales. The line shown here corresponds to the linear fit using all possible measured biased Taylor scales. (b) Y-intercepts obtained through the linear trends of the biased Taylor scales as a function of number of biased Taylor scales used in the fit from (a). The horizontal line represents the average y-intercept, 2.2 ± 0.2 cm. The orange point corresponds the y-intercept of the line in (a).

The subsets are ordered starting with correlations corresponding to the two smallest separations and ending with the entire correlation set. As shown in Fig. 7(a), the biased Taylor scale increases linearly with maximum separation between correlated probes, and it is this trend that will be exploited in the next step.

The second step of the Richardson extrapolation method produces multiple y-intercept values using increasing numbers of points in Fig. 7(a). Each linear fit produces a slightly different y-intercept, plotted in Fig. 7(b). The average of the three points gives a final Taylor scale estimate for these data—2.2 ± 0.2 cm. The error in this estimate is the standard deviation of the three points.

This procedure of obtaining a correlation scale and the Taylor scale is repeated for all shots. The correlation scales are shown in Fig. 8, and Fig. 9 shows the spread of Taylor scales. The average correlation scale is 4.3 ± 1.0 cm, and the average Taylor scale is 2 ± 1 cm.

B. Temporal correlation

Temporal correlations under the Taylor hypothesis are used to estimate the Taylor scale for distances less than the minimum probe separation distance of 2.6 cm. The transformation needs the bulk plasma speed, which is determined experimentally by dividing the probe separation by the average time-delay of prominent features in the unfiltered magnetic field magnitudes. A bulk plasma speed of the plasma plume is determined for each shot. The values range between 19 and 87 km/s.

The temporal correlation functions are constructed with Eq. (4). Figure 10 shows a time-delay correlation of shot 23. As the time-delay increases, the applicability of the Taylor Hypothesis weakens. For this reason, we use the temporal correlations to estimate a Taylor scale but not a correlation scale.

Temporal correlations are converted to spatial correlations and then the Richardson extrapolation method is applied, seen in Sec. II A. Figure 11 shows the Richardson extrapolation on a converted temporal correlation. Figure 11(a) shows the biased Taylor scales based on parabolic fits. Figure 11(b) shows the y-intercepts extracted from the

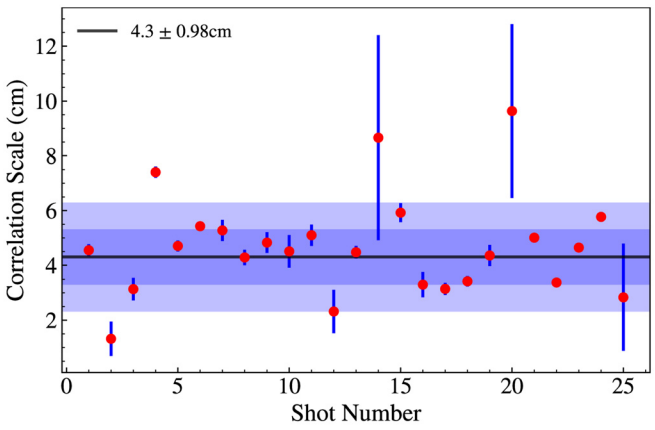

FIG. 8. A scatterplot of correlation scales per shot. The mean is 4.3 ± 1.0 cm, the error is the standard deviation of the points. Shots 2, 14, and 19 are outliers and are excluded from the spatial analysis. The shaded regions correspond to 1 standard deviation (dark blue), and 2 standard deviations (light blue) from the mean value.

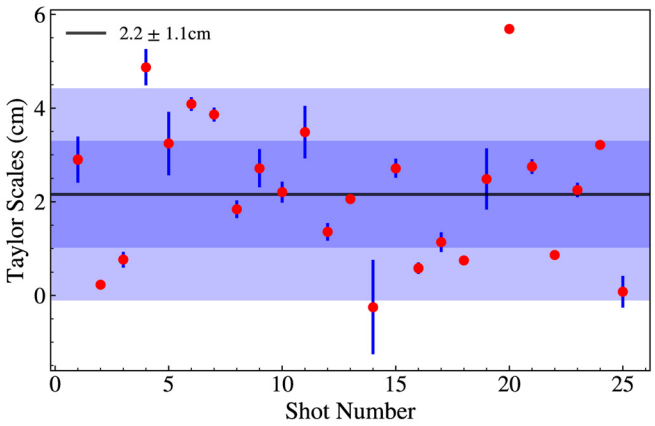

FIG. 9. A scatterplot of Taylor scales from the spatial correlations. The mean is 2 ± 1 cm, the error is the standard deviation of the points. The same shots from Fig. 8 are excluded. The shaded regions correspond to 1 standard deviation (dark blue), and 2 standard deviations (light blue) from the mean value.

biased Taylor scales. There is an inflection point for each shot, occurring near the same transformed spatial point. The cause of this inflection is not understood. However, Chuychai *et al.*[25] suggests the spectral index of the dissipation range within the magnetic power spectrum influences the deviation from a flat trend.

In our case, pending a thorough spectral analysis to address the above point, the best estimate of the Taylor scale is the average value of the full range of the y-intercepts, which corresponds to 2.6 cm away from the probe. For shot 23, the extrapolated Taylor scale is 2.9 ± 0.6 cm. Following this procedure, a Taylor scale is obtained for every shot, shown in Fig. 12. The shot averaged Taylor scale is 3 ± 1 cm.

V. DISCUSSION

The Taylor scale obtained from spatial, 2 ± 1 cm, and temporal, 3 ± 1 cm, correlations are within one standard deviations from each

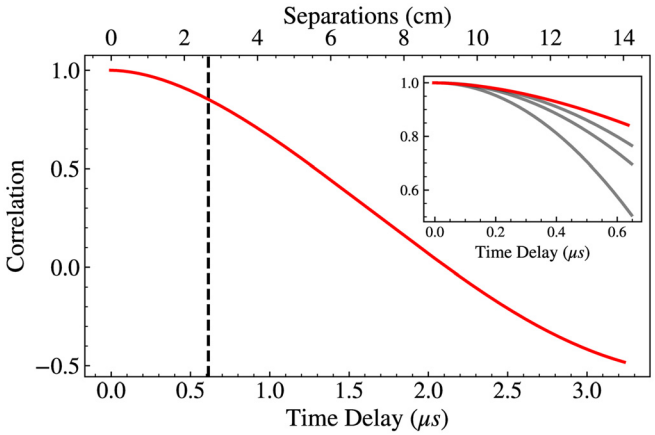

FIG. 10. Temporal correlation of shot 23 of the reference probe. The corresponding spatial separations, via the Taylor Hypothesis, are shown on the top axis. A bulk speed of 40 km/s is found for this shot and used as the conversion factor. The vertical dashed line marks the extent of the inset plot, 0.6 μs or 2.6 cm.

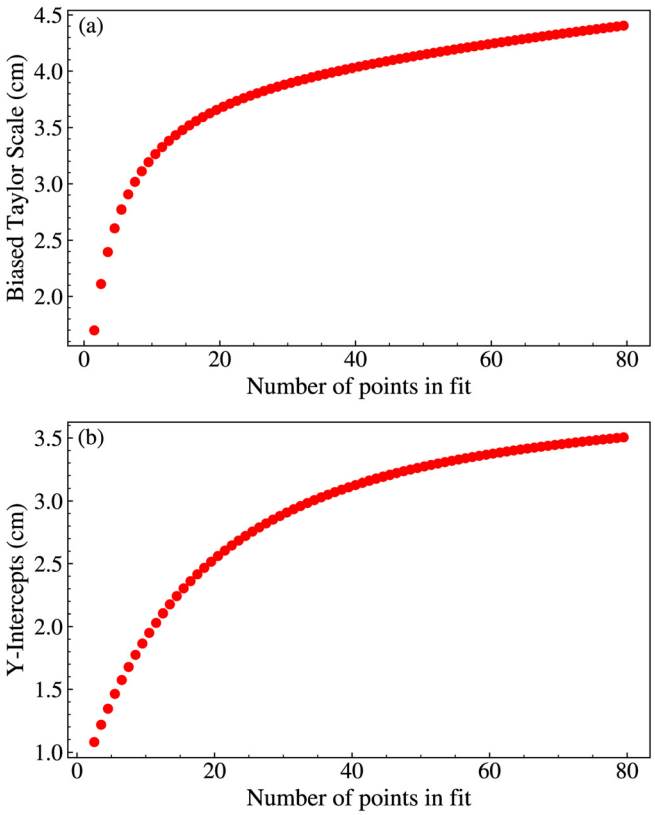

FIG. 11. The Richardson extrapolation on the temporal correlation of shot 23. (a) The biased Taylor scales obtained by fitting Eq. (7) to subsets of the temporal correlation. (b) The y-intercepts of linear fits.

other (Table I). Since the temporal correlation yielded a larger estimate of the Taylor scale than the spatial correlation, it is likely no smaller than 2 ± 1 cm for this plasma. A smaller Taylor scale indicates a larger decorrelation; however, the Taylor scale does not distinguish between

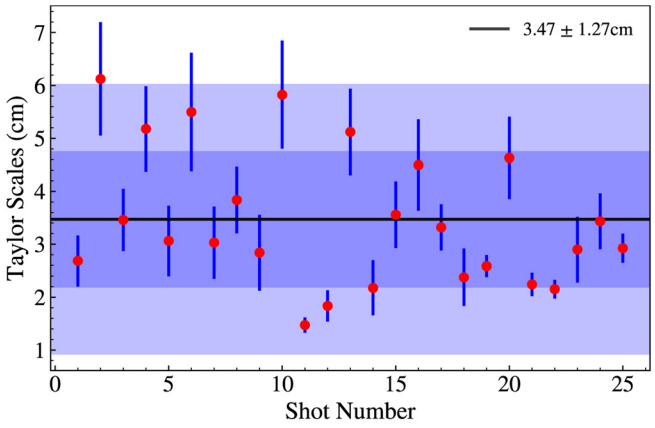

FIG. 12. Taylor scales with respect to shot obtained through the temporal correlations. The mean value is 3 ± 1 cm. The shaded regions correspond to 1 standard deviation (dark blue), and 2 standard deviations (light blue) from the mean value.

TABLE I. The Taylor scales from the spatial and temporal correlations, the correlation scale, and the Taylor magnetic Reynolds number.

	λ_T (cm)	λ_C (cm)	R_m
Spatial	2 ± 1	4.3 ± 1.0	4 ± 1
Temporal	3 ± 1	...	...

the causes of decorrelation and assumes it to be dissipation of energy. We hypothesize that the Taylor scale in plasmas is better understood as an apparent dissipation scale, where non-local energy transfers and various dissipation mechanisms are averaged.

Although this measurement does not prove that dissipation occurs at the Taylor scale, the measured values do fall within estimates of potential dissipation scales computed by other means within the BMX plasma. Based on gas injection and chamber volume, the expected BMX plasma densities are on the order of 2.63×10^{12} to $2.63 \times 10^{14}\,\mathrm{cm}^{-3}$. Thus, ion inertial scales range between 1 and 14 cm. Electron temperature and density predictions, based primarily on similar experiments,[13] give a range of electron mean free paths between 0.5–50 cm. With ion temperature estimates of 20 eV and magnetic field measurements ranging between 400–4000 G, the ion gyroscales range between 0.1–1.0 cm. The Taylor scales measured in this experiment are on the order of these potential dissipation scales, see Table II, but more accurate measurements of plasma parameters are necessary to make any attempts in distinguishing among them. Nevertheless, the fact that a dissipation-relevant scale measurement made with only one diagnostic may be on the right order of magnitude is a promising result and one that encourages experimental refinement.

Another system relevant scale is the $\lambda\,(0.29\,\mathrm{cm}^{-1})$ parameter of the MPGS. The parameter characterizes the linear dimensions of helical magnetic states,[26,27] which self-organize in flux conserving long aspect ratio systems. Normalized to $1/\lambda$, the spatial and temporal Taylor scales are 0.58 and 0.87, respectively, and the correlation scale is 1.2. Although the λ parameter does not quantify a dissipation scale, it quantifies a relative scale natural to the system.[28]

Measurements of the Taylor scale and the correlation scale predict a magnetic Reynolds number no smaller than 4 for this plasma, see Table I. For comparison, a canonical magnetic Reynolds number is computed, given by Eq. (1), using the average axial bulk speed and the MPGS gap of 6.5 cm. The Spitzer resistivity, $\eta_S = 5.2 \times 10^{-5} \frac{ln(\Lambda)}{T_e^{3/2}}$, is $1.6 \times 10^{-5}\,\Omega\,\mathrm{m}$ for a Coulomb logarithm and electron temperature of 10 and 10 eV, where the electron temperature from a similar device is used as a reference.[13] The resulting canonical magnetic Reynolds number is 400. The largest magnetic Reynolds number predicted in this experiment (from a single shot), ~10, is significantly lower than the canonical estimate. Note that the most conservative value for a correlation scale is used, and other potential values, such as the diameter or length of the chamber itself, give larger predictions.

TABLE II. The Taylor scales from the spatial and temporal correlations with different possible normalizations: ion inertial scale (d_i), ion gyro-radius (ρ_i), and the λ ($0.29[\mathrm{cm}^{-1}]$) parameter of the MPGS.

	λ_T/d_i	λ_T/ρ_r	$\lambda_T\lambda$
Spatial	0.14–2	2–20	0.58
Temporal	0.21–3	3–30	0.87

The determination of a reasonable Taylor scale using a single diagnostic technique is encouraging for continuing to refine and study these plasma conditions both experimentally and computationally.

MHD simulations of the BMX plasma using the Pittsburgh Supercomputing Center Bridges-2 machine are in progress. The simulations run on the Dedalus framework,[29] a text-to-code spectral solver. As simulations become more computational expensive with larger Reynolds numbers (due to larger scale separation resolution), the results of this experiment may justify starting with lower magnetic Reynolds number values than anticipated canonical predictions of R_m in order to make comparisons between computation and experiment.

Experimentally, the two primary limiting factors are spatial resolution and applicability of the Taylor Hypothesis. Development of higher spatial resolution measurements is under way. Attaining higher bulk plasma flows is also sought, primarily through increased discharge voltage as well as novel magnetic configurations at the gun. Furthermore, larger shot volumes will allow for increased conditional averaging. Overall, increasing diagnostic variety of the new laboratory will open further detailed comparisons for dissipation mechanisms.

This study does not examine the anisotropic behavior of the magnetic turbulence with respect to fluctuations parallel and perpendicular to the local magnetic field. Nevertheless, we anticipate exploring the anisotropic behavior in future studies.

VI. CONCLUSION

The Taylor scale is a length scale associated with dissipation of energy in turbulent fluid or magnetofluid systems and is used as a means of determining a dissipation scale without the need for measurements of many local parameters. The Taylor scale is measured in the Bryn Mawr Experiment using spatial correlation functions and the Richardson extrapolation procedure. The results yield a Taylor scale of 2 ± 1 cm when measured using spatially separated magnetic pickup probes and 3 ± 1 cm using a single probe and invoking the Taylor Hypothesis. A linear array of pickup probes is also used to determine the correlation scale of this plasma of 4.3 ± 1.0 cm. Combining these metrics, an estimate of the magnetic Reynolds number is made: 4 ± 1. This measured value is smaller than estimates using density and temperature, but if accurate, can significantly help in simulation efforts where smaller magnetic Reynolds numbers require much less computational expense.

ACKNOWLEDGMENTS

This work was supported through a National Science Foundation CAREER Award (No. 1846943).

AUTHOR DECLARATIONS

Conflict of Interest

The authors have no conflicts to disclose.

DATA AVAILABILITY

The data that support the findings of this study are available from the corresponding author upon reasonable request.

REFERENCES

[1]G. K. Batchelor, *The Theory of Homogeneous Turbulence*, Cambridge Science Classics (Cambridge University Press, 1970).
[2]U. Frisch, *Turbulence: The Legacy of A.N. Kolmogorov* (Cambridge University Press, 1995).
[3]H. Belmabrouk and M. Michard, "Taylor length scale measurement by laser Doppler velocimetry," Exp. Fluids **25**, 69–76 (1998).
[4]H. Belmabrouk, "A theoretical investigation of the exactness of Taylor length scale estimates from two-point LDV," Exp. Therm. Fluid Sci. **22**, 45–53 (2000).
[5]W. H. Matthaeus, S. Dasso, J. M. Weygand, L. J. Milano, C. W. Smith, and M. G. Kivelson, "Spatial correlation of solar-wind turbulence from two-point measurements," Phys. Rev. Lett. **95**, 231101 (2005).
[6]J. M. Weygand, W. H. Matthaeus, S. Dasso, M. G. Kivelson, and R. J. Walker, "Taylor scale and effective magnetic Reynolds number determination from plasma sheet and solar wind magnetic field fluctuations," J. Geophys. Res. **112**, A10201, https://doi.org/10.1029/2007JA012486 (2007).
[7]J. M. Weygand, W. H. Matthaeus, S. Dasso, M. G. Kivelson, L. M. Kistler, and C. Mouikis, "Anisotropy of the Taylor scale and the correlation scale in plasma sheet and solar wind magnetic field fluctuations," J. Geophys. Res. **114**, A07213, https://doi.org/10.1029/2008JA013766 (2009).
[8]J. M. Weygand, W. H. Matthaeus, M. El-Alaoui, S. Dasso, and M. G. Kivelson, "Anisotropy of the Taylor scale and the correlation scale in plasma sheet magnetic field fluctuations as a function of auroral electrojet activity," J. Geophys. Res. **115**, A12250, https://doi.org/10.1029/2010JA015499 (2010).
[9]J. M. Weygand, W. H. Matthaeus, S. Dasso, and M. G. Kivelson, "Correlation and Taylor scale variability in the interplanetary magnetic field fluctuations as a function of solar wind speed," J. Geophys. Res. **116**, A08102, https://doi.org/10.1029/2011JA016621 (2011).
[10]R. Bandyopadhyay, W. H. Matthaeus, A. Chasapis, C. T. Russell, R. J. Strangeway, R. B. Torbert, B. L. Giles, D. J. Gershman, C. J. Pollock, and J. L. Burch, "Direct measurement of the solar-wind Taylor microscale using MMS turbulence campaign data," Astrophys. J. **899**, 63 (2020).
[11]M. R. Brown and D. A. Schaffner, "Laboratory sources of turbulent plasma: A unique MHD plasma wind tunnel," Plasma Sources Sci. Technol. **23**, 063001 (2014).
[12]D. A. Schaffner and M. R. Brown, "Multifractal and monofractal scaling in a laboratory magnetohydrodynamic turbulence experiment," Astrophys. J. **811**, 61 (2015).
[13]D. A. Schaffner, V. S. Lukin, A. Wan, and M. R. Brown, "Turbulence analysis of an experimental flux-rope plasma," Plasma Phys. Controlled Fusion **56**, 064003 (2014).
[14]D. A. Schaffner, M. R. Brown, and V. S. Lukin, "Temporal and spatial turbulent spectra of MHD plasma and an observation of variance anisotropy," Astrophys. J. **790**, 126 (2014).
[15]K. T. Osman, W. H. Matthaeus, J. T. Gosling, A. Greco, S. Servidio, B. Hnat, S. C. Chapman, and T. D. Phan, "Magnetic reconnection and intermittent turbulence in the solar wind," Phys. Rev. Lett. **112**, 215002 (2014).
[16]K. G. Klein, G. G. Howes, J. M. TenBarge, and F. Valentini, "Diagnosing collisionless energy transfer using field–particle correlations: Alfvén-ion cyclotron turbulence," J. Plasma Phys. **86**, 905860402 (2020).
[17]K. G. Klein, G. G. Howes, and J. M. TenBarge, "Diagnosing collisionless energy transfer using field-particle correlations: Gyrokinetic turbulence," J. Plasma Phys. **83**, 535830401 (2017).
[18]W. H. Matthaeus, J. M. Weygand, P. Chuychai, S. Dasso, C. W. Smith, and M. G. Kivelson, "Interplanetary magnetic Taylor microscale and implications for plasma dissipation," Astrophys. J. **678**, L141–L144 (2008).
[19]G. I. Taylor, "Statistical theory of turbulenc," Proc. R. Soc. A. **151**, 421–444 (1935).
[20]A. Shalchi, "Perpendicular transport of energetic particles in magnetic turbulence," Space Sci. Rev. **216**, 23 (2020).
[21]Y. Kaneda, "Lagrangian and Eulerian time correlations in turbulence," Phys. Fluids A **5**, 2835–2845 (1993).
[22]G. I. Taylor, "The spectrum of turbulence," Proc. R. Soc. A **164**, 476–490 (1938).
[23]C. G. R. Geddes, T. W. Kornack, and M. R. Brown, "Scaling studies of spheromak formation and equilibrium," Phys. Plasmas **5**, 1027 (1997).
[24]C. H. K. Chen, "Recent progress in astrophysical plasma turbulence from solar wind observations," J. Plasma Phys. **82**, 535820602 (2016).
[25]P. Chuychai, J. M. Weygand, W. H. Matthaeus, S. Dasso, C. W. Smith, and M. G. Kivelson, "Technique for measuring and correcting the Taylor microscale," J. Geophys. Res. **119**, 4256–4265, https://doi.org/10.1002/2013JA019641 (2014).
[26]C. D. Cothran, M. R. Brown, T. Gray, M. J. Schaffer, and G. Marklin, "observation of a helical self-organized state in a compact toroidal plasma," Phys. Rev. Lett. **103**, 215002 (2009).
[27]T. Gray, M. R. Brown, and D. Dandurand, "Observation of a relaxed plasma state in a quasi-infinite cylinder," Phys. Rev. Lett. **110**, 085002 (2013).
[28]P. M. Bellan, *Spheromaks a Practical Application of Magnetohydrodynamic Dynamos and Plasma Self-Organization* (Imperial College Press, London, 2000).
[29]K. J. Burns, G. M. Vasil, J. S. Oishi, D. Lecoanet, and B. P. Brown, "Dedalus: A flexible framework for numerical simulations with spectral methods," Phys. Rev. Res. **2**, 023068 (2020).